HEFAT2008
6th International Conference on Heat Transfer, Fluid Mechanics and Thermodynamics
30 June to 2 July 2008
Pretoria, South Africa
Paper number: CM3

NATURAL CONVECTION INSIDE ENCLOSURES PARTIALLY HEATED AT ONE SIDE

M. Corcione *, L. Fontana and E. Habib
*Author for correspondence
Dipartimento di Fisica Tecnica, "Sapienza" University of Rome
via Eudossiana, 18 – 00184 Rome, Italy
e-mail: massimo.corcione@uniroma1.it

ABSTRACT

Steady laminar natural convection heat transfer inside air-filled square cavities cooled at one side and partially heated at the opposite side, is studied numerically. A computational code based on SIMPLE-C algorithm is used for the solution of the mass, momentum, and energy transfer equations. Simulations are performed for different values of the dimensionless size and location of the heater, and the Rayleigh number, whose effects on the temperature and velocity fields, and on the heat transfer rate across the cavity, are analyzed and discussed.

INTRODUCTION

Natural convection heat transfer inside rectangular cavities with differentially heated sides has been extensively studied, being of interest in diverse engineering applications, e.g., heat removal from electronic equipment, solar energy collection, and heat transfer in buildings. However, in many practical cases heating takes place just over a portion of one of the sidewalls, whose size and location may affect significantly the amount of heat transferred across the enclosure.

Natural convection inside air-filled rectangular enclosures partially heated at one side was studied first by Chu et al. [1], who conducted a parametric investigation aimed at determing the effects of the heater size and location, as well as those of the aspect ratio of the cavity, on the rate of heat transfer and fluid circulation. More recently, three-dimensional numerical studies were conducted by Frederick and Quiroz [2], on air-filled cubical enclosures with a cold vertical wall and a hot square sector located in the center of the opposite wall, and by He et al. [3], on liquid-filled cubical enclosures with a cold vertical wall and two square isothermal heaters located one above the other on the opposite wall. In addition, recent papers with a bearing on this topic are those performed by Deng et al. [4], and by Chen and Chen [5], on air-filled square cavities cooled at one side and discretely heated at the opposite side and at the bottom.

Actually, since none of these studies contains a general correlating-equation for predicting the thermal performance of the system, the scope of the present paper is to carry out a study of natural convection inside square cavities cooled at one side and partially heated at the other side by an isothermal heater of variable length and position, in order to derive a heat transfer correlation spanning across ranges of the independent variables sufficiently wide to be of interest for applications.

The study is conducted numerically under the assumption of two-dimensional laminar flow. A computer code based on the SIMPLE-C algorithm is employed for the solution of the mass, momentum and energy conservation equations. Simulations are performed for air and different values of the dimensionless size and location of the heater, and the Rayleigh number based on the cavity width, whose effects on the flow and temperature fields, as well as on the heat transfer rates, are analyzed in full detail and discussed.

MATHEMATICAL FORMULATION

An air-filled square enclosure of width W is considered. The coordinate system is defined so that the x-axis is horizontal, while the y-axis is vertical and pointing upwards.

The cavity is cooled at one side, and partially heated at the opposite side. The discrete heat source, of length L, whose center is located at a distance d from the bottom endwall of the enclosure, is kept at uniform temperature T_H, while the cooled side is maintained at temperature T_C. The remaining upper and lower parts of the heated sidewall, as well as the top and bottom endwalls of the cavity, are considered perfectly insulated, as depicted in Fig. 1, where the (x,y) coordinate system adopted is also represented.

The flow is assumed to be two-dimensional, laminar and incompressible, with constant fluid properties and negligible viscous dissipation and pressure work. The buoyancy effects on momentum transfer are taken into account by the Boussinesq approximation.

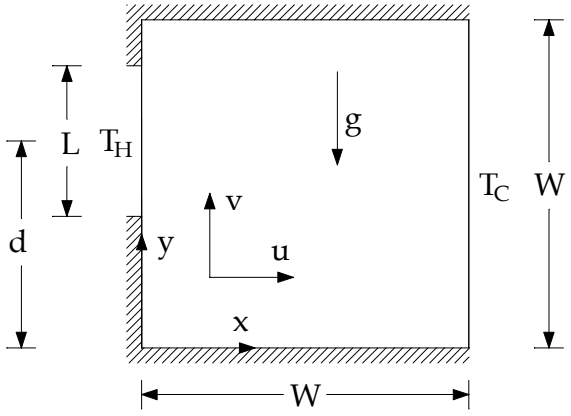

Figure 1 – Sketch of the geometry and coordinate system

Once the above assumptions are used in the conservation equations of mass, momentum and energy, and the following dimensionless variables are introduced:

$$X = \frac{x}{W} \qquad Y = \frac{y}{W} \qquad \tau = \frac{t}{\left(W^2/\nu\right)} \tag{1}$$

$$U = \frac{u}{\left(\nu/W\right)} \qquad V = \frac{v}{\left(\nu/W\right)} \qquad P = \frac{p + \rho g y}{\rho\left(\nu/W\right)^2} \tag{2}$$

$$\theta = \frac{\left(T - T_C\right)}{\left(T_H - T_C\right)} \tag{3}$$

the following set of governing equations is obtained:

$$\frac{\partial U}{\partial X} + \frac{\partial V}{\partial Y} = 0 \tag{4}$$

$$\frac{\partial U}{\partial \tau} + U\frac{\partial U}{\partial X} + V\frac{\partial U}{\partial Y} = -\frac{\partial P}{\partial X} + \left(\frac{\partial^2 U}{\partial X^2} + \frac{\partial^2 U}{\partial Y^2}\right) \tag{5}$$

$$\frac{\partial V}{\partial \tau} + U\frac{\partial V}{\partial X} + V\frac{\partial V}{\partial Y} = -\frac{\partial P}{\partial Y} + \left(\frac{\partial^2 V}{\partial X^2} + \frac{\partial^2 V}{\partial Y^2}\right) + \frac{Ra}{Pr}\theta \tag{6}$$

$$\frac{\partial \theta}{\partial \tau} + U\frac{\partial \theta}{\partial X} + V\frac{\partial \theta}{\partial Y} = \frac{1}{Pr}\left(\frac{\partial^2 \theta}{\partial X^2} + \frac{\partial^2 \theta}{\partial Y^2}\right) \tag{7}$$

In the above equations u and v are the velocity components along x and y, respectively, i.e., horizontal and vertical; t is the time; T is the temperature; p is the pressure; ρ is the density; g is the acceleration of gravity; ν is the kinematic viscosity; Pr is the Prandtl number; and Ra is the Rayleigh number defined as:

$$Ra = \frac{g\beta(T_H - T_C)W^3}{\nu^2}Pr \tag{8}$$

Other parameters which enter into this study are:

(a) the dimensionless size of the heater

$$E = \frac{L}{W} \qquad 0.2 \le E \le 1 \tag{9}$$

(b) the dimensionless location of the heater

$$D = \frac{d}{W} \qquad E/2 \le D \le 1 - E/2 \tag{10}$$

The boundary conditions assumed are the no-slip condition U = V = 0 at the four boundary walls, and θ = 1 and θ = 0 at the heated and cooled surfaces, respectively.

The initial conditions assumed are fluid at rest, i.e., U = V = 0, and uniform temperature θ = 0 throughout the whole cavity.

COMPUTATIONAL PROCEDURE

The set of governing equations (4)–(7) with the boundary and initial conditions stated above is solved through a control-volume formulation of the finite-difference method.

The coupling of velocity and pressure is handled through the SIMPLE-C algorithm by Van Doormaal and Raithby [6]. The QUICK discretization scheme by Leonard [7] is used for the evaluation of the interface advection fluxes. A second-order backward scheme is used for time stepping.

Starting from the assigned initial fields of the dependent variables across the cavity, at each time-step the discretized governing equations are solved iteratively through a line-by-line application of the Thomas algorithm, enforcing under-relaxation for convergence.

The computational spatial domain is covered with a non-uniform grid, having a concentration of grid lines near the boundary walls and both ends of the heat source, and a uniform spacing throughout the remainder interior of the cavity. Time discretization is chosen uniform. Within each time step, the spatial solution is considered to be fully converged when the maximum absolute values of both the mass source and the percentage changes of the dependent variables at any grid-node from iteration to iteration are smaller than the prescribed values, i.e., 10^{-4} and 10^{-5}, respectively.

Time-integration is stopped once steady-state is reached. This means that the simulation procedure ends when the percentage difference between the incoming and outgoing heat transfer rates, and the percentage changes of the time-derivatives of the dependent variables at any grid-node between two consecutive time-steps, are smaller than the prescribed values, i.e., 10^{-6} and 10^{-7}, respectively.

Once steady-state is reached, the average Nusselt numbers Nu_H and Nu_C of the heater and the cooled wall, respectively, are calculated:

$$Nu_H = \frac{h_H W}{k} = \frac{Q_{in} W}{kL\left(T_H - T_C\right)} =$$

$$= \frac{1}{E}\cdot\frac{Q_{in}}{k\left(T_H - T_C\right)} = -\frac{1}{E}\int_{D-E/2}^{D+E/2}\left.\frac{\partial\theta}{\partial X}\right|_{X=0} dY \tag{11}$$

$$Nu_C = \frac{h_C W}{k} = \frac{Q_{out} W}{kW(T_C - T_H)} =$$

$$= \frac{Q_{out}}{k(T_C - T_H)} = -\int_0^1 \left.\frac{\partial\theta}{\partial X}\right|_{X=1} dY \qquad (12)$$

where h_H and h_C are the average coefficients of convection of the heater and the cooled sidewall, respectively, and Q_{in} and Q_{out} are the overall incoming and outgoing heat transfer rates added to the fluid by the heater and withdrawn from the fluid by the cooled sidewall, respectively. The temperature gradients at any active boundary surface are evaluated by a second-order profile among each wall-node and the next two corresponding fluid-nodes.

Of course, since at steady-state the incoming and outgoing heat transfer rates are the same, that is, $Q_{in} = -Q_{out} = Q$, the following relationship between Nu_H and Nu_C holds:

$$Nu_H = \frac{Nu_C}{E} \qquad (13)$$

Tests on the dependence of the results on both grid-size and time-step have been performed for several combinations of the independent variables E, D and Ra. The optimal grid-size and time-step used for computations, which represent a good compromise between solution accuracy and computational time required, are such that further refinements do not yield for noticeable modifications neither in the heat transfer rates nor in the flow field, that is, the percentage difference between the first and the second members of eq. (13), and the percentage changes of the maximum horizontal and vertical velocity components on the midplanes of the enclosure, are smaller than the prescribed accuracy values, i.e., 1% and 2%, respectively. Typically, the number of nodal points and the time step used for computations lie in the ranges between 40×40 and 80×400, and between 10^{-6} and 10^{-3}, respectively.

Moreover, some test runs have also been executed with the initial uniform dimensionless temperature of the fluid set to 0.5 or 1, in order to determine the effect of the initial conditions on the steady-state flow and temperature fields. Indeed, solutions practically identical to those obtained for $\theta = 0$ were obtained for all the configurations examined.

Finally, in order to validate the numerical code used for the present study, the steady-state solutions obtained for $\tau \to \infty$ in a square cavity with differentially heated sidewalls and adiabatic top and bottom endwalls for Rayleigh numbers from 10^3 to 10^6, have been compared with the benchmark data of de Vahl Davis [8]. In particular, the average Nusselt numbers as well as the maximum horizontal and vertical velocity components, on the vertical and horizontal midplanes, respectively, are well within 1% of the benchmark data, as reported in Table 1. It is worth noticing that our dimensionless velocity results have been multiplied by the Prandtl number before being inserted in Table 1, so as to account for the choice of the ratio between kinematic viscosity and characteristic length of the cavity as scale factor for the velocity, instead of the ratio between thermal diffusivity and characteristic length, used in ref. [8]. More details on the code validation are available in Cappelli D'Orazio et al. [9].

Table 1 – Comparison of thermally-driven square cavity solutions

Ra		U_{max}	V_{max}	Nu_{av}
10^3	Present	3.654	3.708	1.116
	Benchmark [8]	3.649	3.697	1.118
10^4	Present	16.242	19.714	2.254
	Benchmark [8]	16.178	19.617	2.243
10^5	Present	35.008	68.109	4.506
	Benchmark [8]	34.722	68.590	4.519
10^6	Present	65.226	221.598	8.879
	Benchmark [8]	64.630	219.360	8.800

RESULTS AND DISCUSSION

Numerical simulations are performed for Pr = 0.71, which corresponds to air, and different values of the dimensionless size of the heater, E, in the range between 0.2 and 1, the dimensionless location of the heater, D, in the range between E/2 and (1 − E/2), and the Rayleigh number of the enclosure, Ra, in the range between 10^3 and 10^7.

A selection of local results is presented in Figs. 2–11, where isotherm contours, corresponding to equispaced values of θ in the range between 0 and 1, are plotted for different sets of values of E, D, and Ra, in order to highlight the effects of any independent variable on the temperature field, and then on the amount of heat exchanged at the heater surface. In particular, the effects of E and Ra are pointed out in Figs. 2–6, which are referred to D = 0.5, while those of D and Ra are illustrated in Figs. 7–11, which are referred to E = 0.2.

As regards the fluid motion, the corresponding streamline plots are omitted for the sake of brevity. Indeed, as expected, for all the configurations examined the flow field consists of a single roll-cell which derives from the rising of the hot fluid adjacent to the heater and its descent along the opposite cooled sidewall. Indications on the rate of fluid circulation are reported in Tables 2–3 in terms of $|\psi|_{max}$, i.e., the maximum absolute value of the dimensionless stream function, defined as usual through $U = \partial\Psi/\partial Y$ and $V = -\partial\Psi/\partial X$.

As far as the overall results are concerned, the heat transfer performance of the cavity is expressed in terms of the average Nusselt number of the cooled wall Nu_C, which is considered more suitable for this purpose than that of the heater Nu_H. In fact, once both Ra and D are assigned, the amount Q of heat transferred across the cavity obviously increases as the length E of the heater increases. Correspondingly, a Nusselt number which would represent the thermal behavior of the cavity "at a glance" should increase with increasing E. On the other hand, according to eq. (11), it is $Nu_H \sim Q/E$, thus implying that Nu_H may either increase or decrease with increasing E, depending on whether $\partial Q/\partial E$ is positive or negative. In contrast, based on eq. (12), it is $Nu_C \sim Q$, which means that Nu_C unequivocally increases with E. Moreover, the Nusselt number Nu_C coincides with the average Nusselt number of the heater Nu* when its size L is used as characteristic length instead of the width W of the cavity:

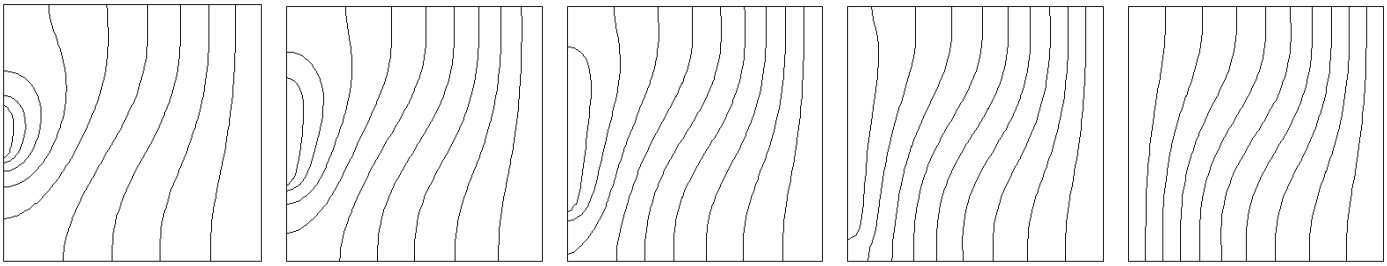

Figure 2 – Isotherm lines for Ra = 10^3, D = 0.5, and E = 0.2, 0.4, 0.6, 0.8, 1.0

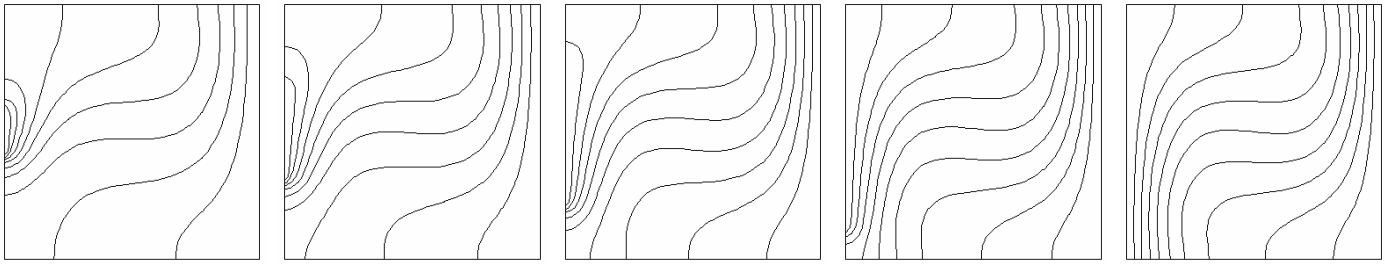

Figure 3 – Isotherm lines for Ra = 10^4, D = 0.5, and E = 0.2, 0.4, 0.6, 0.8, 1.0

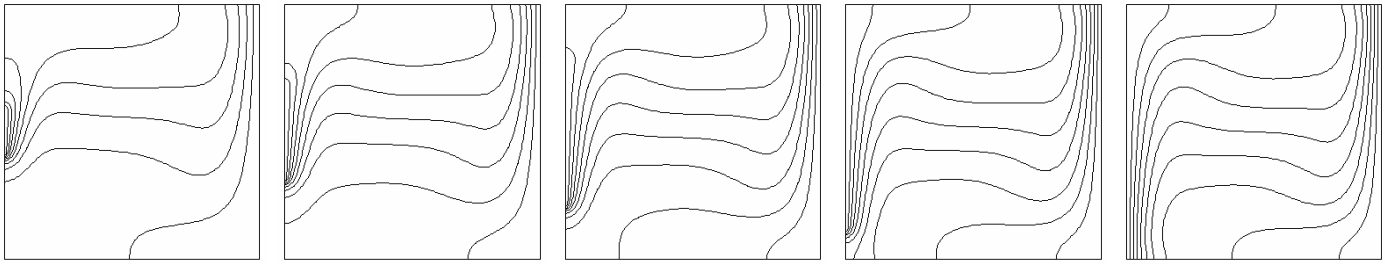

Figure 4 – Isotherm lines for Ra = 10^5, D = 0.5, and E = 0.2, 0.4, 0.6, 0.8, 1.0

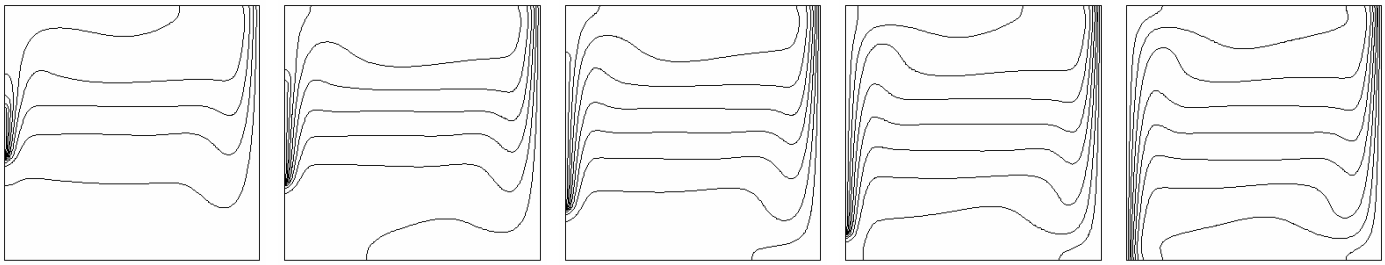

Figure 5 – Isotherm lines for Ra = 10^6, D = 0.5, and E = 0.2, 0.4, 0.6, 0.8, 1.0

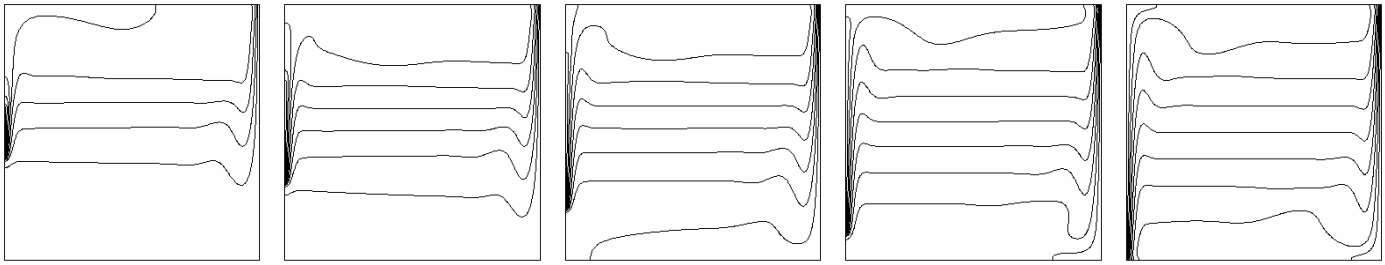

Figure 6 – Isotherm lines for Ra = 10^7, D = 0.5, and E = 0.2, 0.4, 0.6, 0.8, 1.0

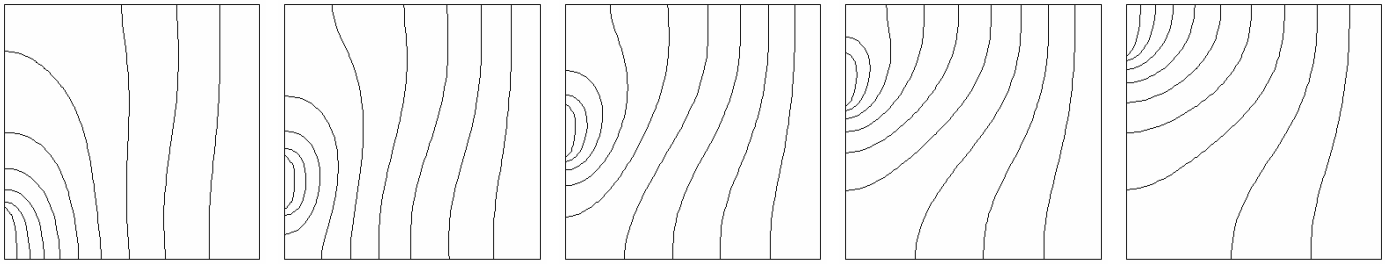

Figure 7 – Isotherm lines for Ra = 10^3, E = 0.2, and D = 0.1, 0.3, 0.5, 0.7, 0.9

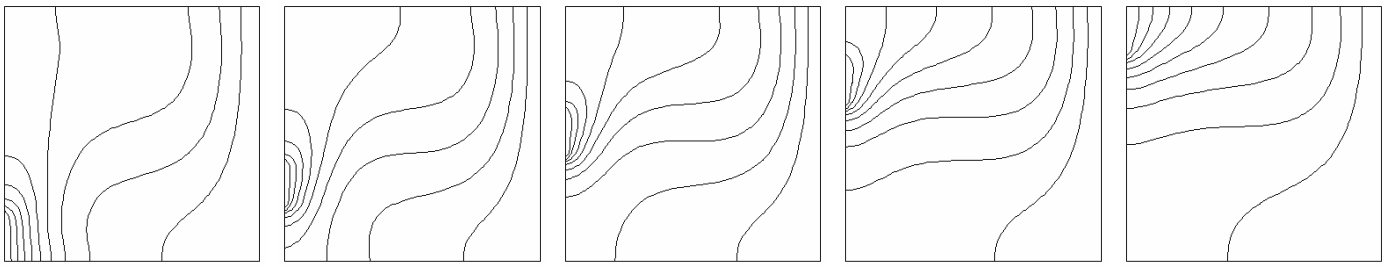

Figure 8 – Isotherm lines for Ra = 10^4, E = 0.2, and D = 0.1, 0.3, 0.5, 0.7, 0.9

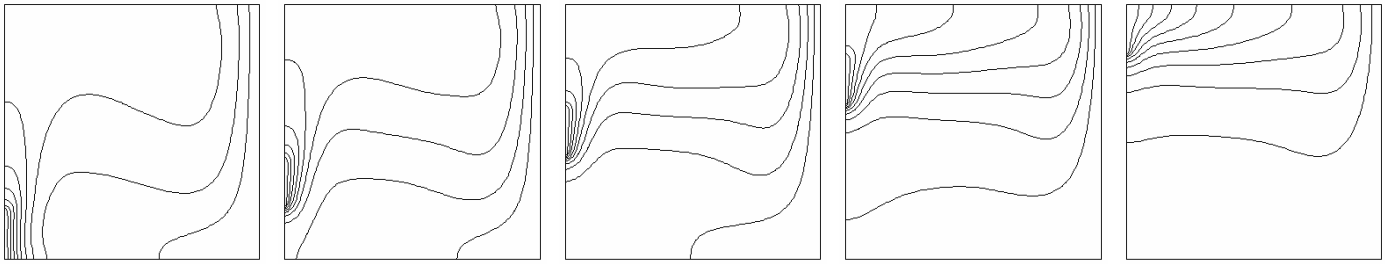

Figure 9 – Isotherm lines for Ra = 10^5, E = 0.2, and D = 0.1, 0.3, 0.5, 0.7, 0.9

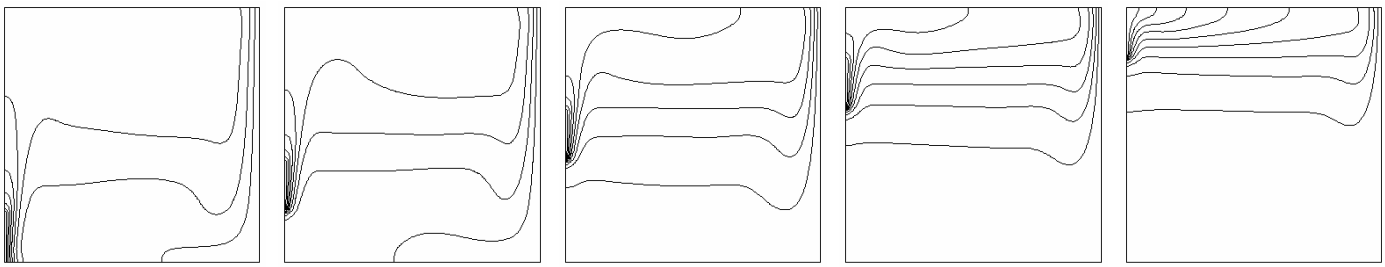

Figure 10 – Isotherm lines for Ra = 10^6, E = 0.2, and D = 0.1, 0.3, 0.5, 0.7, 0.9

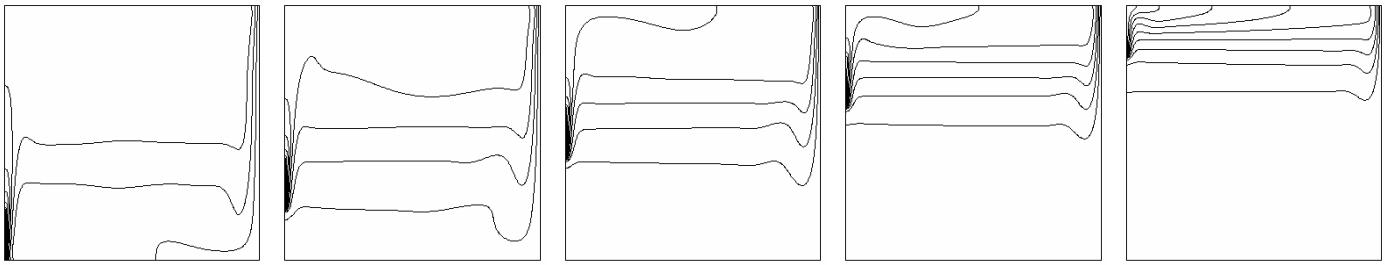

Figure 11 – Isotherm lines for Ra = 10^7, E = 0.2, and D = 0.1, 0.3, 0.5, 0.7, 0.9

Table 2 – $|\Psi|_{max}$ for D = 0.5, Ra = 10^3 to 10^7 and E = 0.2 to 1

D = 0.5	$\|\psi\|_{max}$				
Ra	E = 0.2	0.4	0.6	0.8	1
10^3	1.26	1.46	1.57	1.62	1.64
10^4	5.47	6.19	6.68	6.98	7.09
10^5	10.16	11.33	12.33	13.12	13.45
10^6	20.66	21.77	21.79	22.56	23.53
10^7	39.69	40.24	38.21	39.81	42.23

Table 3 – $|\Psi|_{max}$ for E = 0.2, Ra = 10^3 to 10^7 and D = 0.1 to 0.9

E = 0.2	$\|\psi\|_{max}$				
Ra	D = 0.1	0.3	0.5	0.7	0.9
10^3	1.02	1.47	1.26	1.08	0.82
10^4	5.93	6.35	5.47	4.30	3.38
10^5	14.81	13.43	10.16	8.00	6.38
10^6	29.82	26.17	20.66	13.93	10.12
10^7	59.73	49.44	39.69	27.96	16.03

$$Nu^* = \frac{h_H L}{k} = \frac{Q_{in} L}{kL(T_H - T_C)} = E \cdot Nu_H = Nu_C \qquad (14)$$

which actually delivers a better information on the effectiveness of heat removal from the heater rather than Nu_H.

Distributions of $Nu^* \equiv Nu_C$ are plotted against the Rayleigh number Ra in Figs. 12 and 13, for D = 0.5 and E = 0.2, 0.6, and 1, and for E = 0.2 and D = 0.1, 0.5, and 0.9, respectively. It may be noticed that the heat transfer performance of the enclosure increases with Ra and E, while showing a peak for intermediate values of D, as pointed out in Fig. 14, where the distributions of $Nu^* \equiv Nu_C$ vs. D are reported for E = 0.2 (that may be considered of major interest for applications, since usually the size of the heater is sufficiently smaller than the characteristic length of its enclosure) and different values of Ra.

The existence of an optimum position of the heater for maximum heat removal may be explained by considering that when the heater is located too close to either the bottom or the top wall of the enclosure, the amount of heat exchanged by its lower portion or upper portion, respectively, is smaller than that correspondingly exchanged when the heater is located in the middle of the wall, as the rising jet of fluid cannot wash the entire surface of the heater. This is, e.g., shown in Fig. 15 where the distributions of the local Nusselt number along the heater surface $[-(\partial\theta/\partial X)]_{X=0}$ are plotted for Ra = 10^5, E = 0.2, and different values of D.

All the values obtained for the optimum position D_{opt} of the heater for $E \le 0.6$ and $10^3 \le Ra \le 10^7$ may be correlated to E and Ra through the following monomial equation:

$$D_{opt} = 0.593\left(Ra / E^{1.5}\right)^{-0.029} \qquad (15)$$

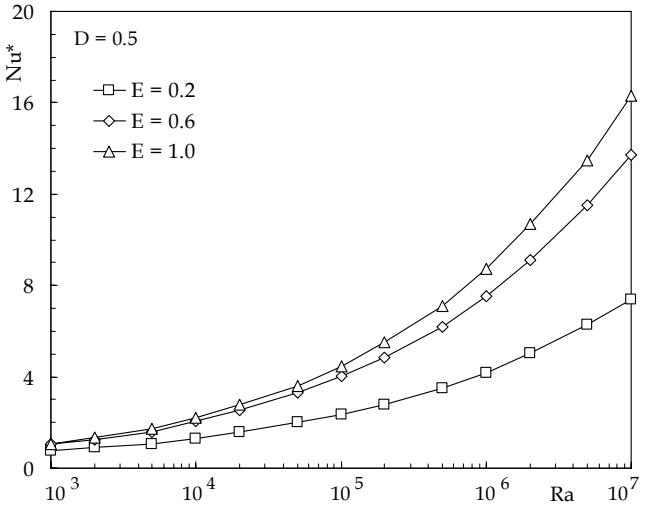

Figure 12 – Distributions of Nu* vs. Ra for D = 0.5 and different values of the dimensionless size of the heater E

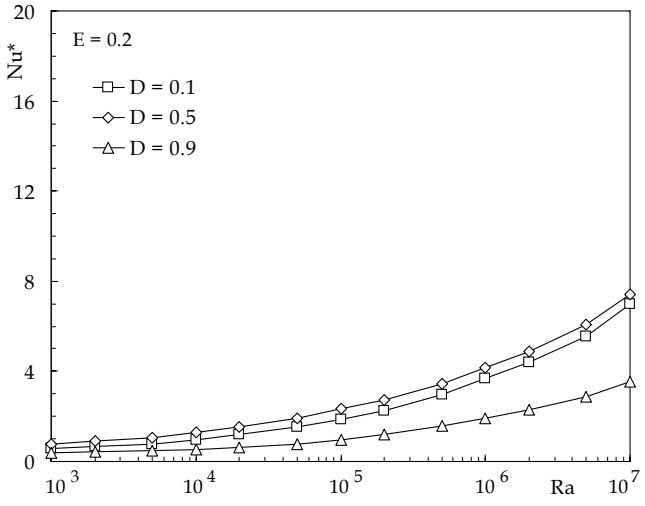

Figure 13 – Distributions of Nu* vs. Ra for E = 0.2 and different values of the dimensionless location of the heater D

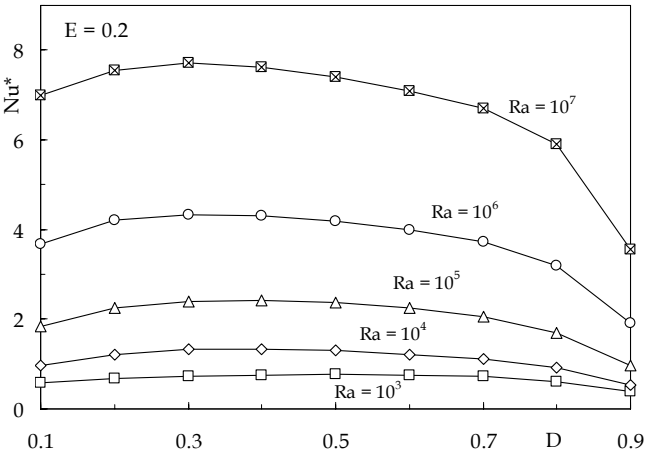

Figure 14 – Distributions of Nu* vs. D for E = 0.2 and different values of the Rayleigh number Ra

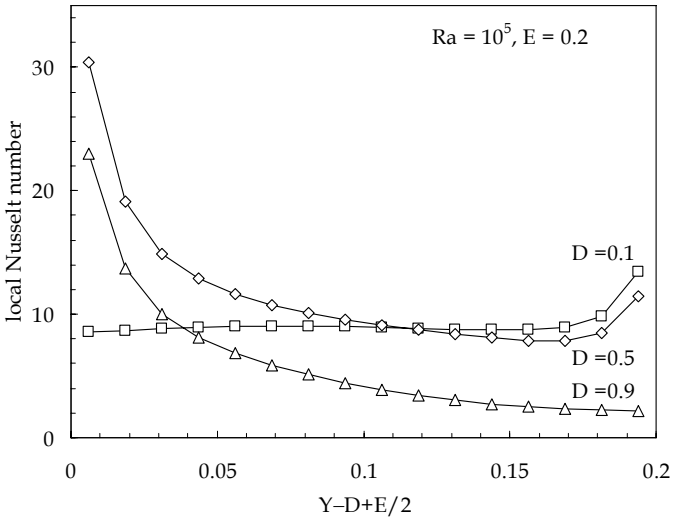

Figure 15 – Distributions of the local Nusselt number along the heater for $Ra = 10^5$, $E = 0.2$ and different values of D

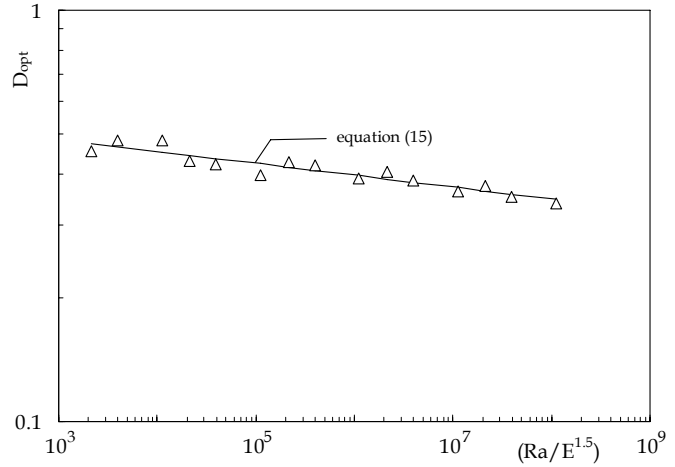

Figure 16 – Comparison between equation (15) and the numerical results obtained for D_{opt}

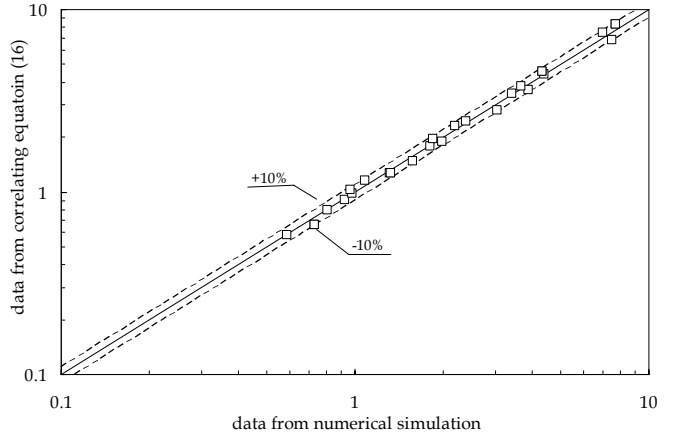

Figure 17 – Comparison between the Nusselt numbers predicted by equations (16)–(19) and those derived from the numerical simulations.

with a 3.6% standard deviation of error and a ±6.4% range of error, as shown in Fig. 16.

Finally, the numerical results obtained for $Nu^* \equiv Nu_C$ may be expressed as a function of the independent variables Ra, E and D through the following semi-empirical correlations:

- for $D \le D_{opt}$ and $E \le 0.6$, and $10^3 \le Ra \le 10^7$

$$Nu^* = \left[A_D (\log Ra)^2 + B_D (\log Ra) + C_D\right]\left(Ra \cdot E^{1.5}\right)^{0.25} \quad (16)$$

where

$$A_D = 0.03(D_{opt} - D) - 0.005 \quad (17)$$

$$B_D = -0.3(D_{opt} - D) + 0.06 \quad (18)$$

$$C_D = 0.5(D_{opt} - D) + 0.1 \quad (19)$$

with a 5.9% standard deviation of error and a range of error from –9.5% to + 7.3%, as shown in Fig. 17;

- for ($D > D_{opt}$ and $E \le 0.6$) or $E > 0.6$, and $10^3 < Ra \le 10^7$

$$Nu^* = \left[0.19Ra^{0.027} - 0.68(D - D_{opt})Ra^{-0.01}\right]\left(Ra \cdot E^{1.5}\right)^{0.25} \quad (20)$$

with a 4.6% standard deviation of error and a range of error from –8.6% to + 10%, as shown in Fig. 18.

Note that the value for D_{opt} to be employed in eqs. (17)–(20) is the one obtained by eq. (15). In particular, this holds true also for $E > 0.6$, which implies the use of eq. (20), although eq. (15) is applicable only for $E \le 0.6$ – it is plain that the value of D_{opt} derived from eq. (15) for $E > 0.6$ has the only scope to calculate Nu* through eq. (20), ceasing completely to have the meaning of optimum position of the heater for maximum heat removal.

CONCLUSIONS

Steady laminar natural convection heat transfer inside air-filled square cavities cooled at one side and partially heated at the opposite side, has been studied numerically. Simulations

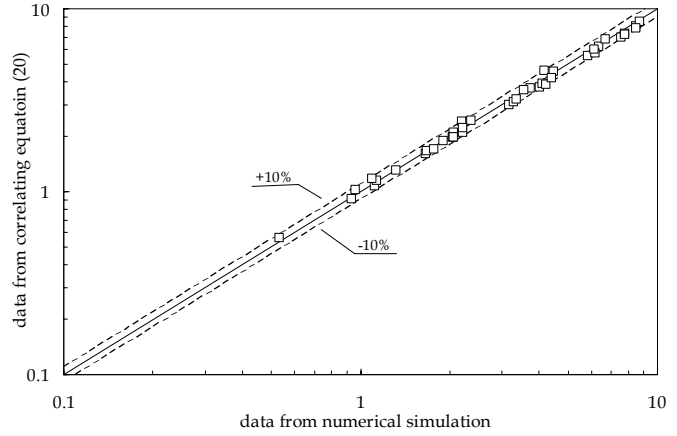

Figure 18 – Comparison between the Nusselt numbers predicted by equation (20) and those derived from the numerical simulations.

have been performed for different values of the dimensionless size of the heater E (i.e., the ratio between the length of the heater and the width of the cavity) in the range between 0.2 and 1, the dimensionless location of the heater D (i.e. the ratio between the distance of the center of the heater from the bottom endwall of the cavity and the width of the cavity) in the range between E/2 and (1 – E/2), and the Rayleigh number Ra of the cavity, based on its width, in the range between 10^3 and 10^7.

It has been found that the heat transfer performance of the cavity increases with increasing the Rayleigh number and the size of the heater. As far as the heater location is concerned, the amount of heat transferred across the enclosure has a peak for intermediate positions, the higher is the Rayleigh number, the closer to the bottom endwall of the enclosure is such optimum location of the heater for maximum heat removal.

NOMENCLATURE

D dimensionless location of the heater = d/W
d distance of the center of the heater from the bottom wall
E dimensionless size of the heater = L/W
g gravitational acceleration
h average coefficient of convection
L length of the heater
Nu average Nusselt number based on W = hW/k
Nu* average Nusselt number based on L = hL/k
P dimensionless pressure
p pressure
Pr Prandtl number = ν/α
Q heat transfer rate
Ra Rayleigh number = $g\beta(T_H - T_C)W^3Pr/\nu^2$
T temperature
t time
U dimensionless horizontal velocity component
u horizontal velocity component
V dimensionless vertical velocity component
v vertical velocity component
W width of the cavity
X dimensionless horizontal coordinate
x horizontal coordinate
Y dimensionless vertical coordinate
y vertical coordinate

Greek symbols

α thermal diffusivity of the fluid
β coefficient of volumetric thermal expansion of the fluid
ν kinematic viscosity of the fluid
θ dimensionless temperature
ρ density of the fluid
τ dimensionless time
ψ dimensionless stream function

Subscripts

C cold
H hot
max maximum value

REFERENCES

[1] H. H. S. Chu, S. W. Churchill, C. V. S. Patterson, The effect of heater size, location, aspect ratio, and boundary conditions on two-dimensional, laminar, natural convection in rectangular channels, J. Heat Transfer 98 (1976) 194-201.

[2] R. L. Frederick, F. Quiroz, On the transition from conduction to convection regime in a cubical enclosure with a partially heated wall, Int. J. Heat Mass Transfer 44 (2001) 1699-1709.

[3] Y. L. He, W. W. Yang, W. Q. Tao, Three-dimensional numerical study of natural convective heat transfer of liquid in a cubic enclosure, Num. Heat Transfer 47 (2005) 917-934.

[4] Q. H. Deng, G. F. Tang, Y. Li, A combined temperature scale for analyzing natural convection in rectangular enclosures wth discrete wall heat sources, Int. J. Heat Mass Transfer 45 (2002) 3437-3446.

[5] T. H. Chen, L. Y. Chen, Study of buoyancy-induced flows subjected to partially heated sources on the left and bottom walls in a square enclosure, Int. J. Thermal Sciences 46 (2007) 1219-1231.

[6] J. P. Van Doormaal and G. D. Raithby, Enhancements of the simple method for predicting incompressible fluid flows, Num. Heat Transfer 11 (1984) 147-163.

[7] B. P. Leonard, A stable and accurate convective modelling procedure based on quadratic upstream interpolation, Comp. Meth. in Appl. Mech. Engng. 19 (1979) 59-78.

[8] G. de Vahl Davis, Natural convection of air in a square cavity: a bench mark numerical solution, Int. J. Num. Meth. Fluids 3 (1983) 249–264.

[9] M. Cappelli D'Orazio, C. Cianfrini, M. Corcione, Rayleigh-Bénard convection in tall rectangular enclosures, Int. J. Thermal Sciences 43 (2004) 135-144.